

Local and global effects of Mg^{2+} on Ago and miRNA-target interactions

Zhi Ma · Zhenghua Xue · Huixiao Zhang · Yan Li ·
Yonghua Wang

Received: 6 August 2011 / Accepted: 6 February 2012 / Published online: 7 March 2012
© Springer-Verlag 2012

Abstract Three magnesium ions (Mg^{2+}), named Mg1 (in Mid domain), Mg2 and Mg3 (both in PIWI domain), located at the small RNA binding domain of Argonaute (Ago) protein, are important for sequence-specific miRNA-target interactions. Such conjunction between the Ago protein and miRNA raises the question: How do Mg^{2+} ions participate in the recognition process of miRNA by Ago or its target. Furthermore, it is still unclear whether the Mg^{2+} ions contribute to the local or global stability of the miRNA complex. In this work, we have performed a series of 16 independent molecular dynamic simulations (MD) to characterize the functions of Mg^{2+} , hydration patterns and the conformational events involved in the miRNA-target interactions. The cross correlation analysis shows that Mg1 and Mg2 significantly enhance a locally cooperated movement of the PAZ, PIWI and Mid domains with the average correlation coefficient of ~ 0.65 ,

producing an “open-closed” motion (rotation Angle, 46.5°) between the PAZ and PIWI domains. Binding of Mg3 can globally stabilize the whole Ago protein with the average RMSD of ~ 0.34 Å, compared with the systems in absence of Mg3 (average RMSD ~ 0.43 Å). Three structural water molecules surrounding the Mg^{2+} -binding regions also stabilize these ions, thus facilitating the recognition of miRNA to its target. In addition, the thermodynamic analysis also verifies the positive contribution of all three Mg^{2+} to the binding of miRNA to Ago, as well as the importance Mg2 plays in the cleavage of the miRNA targets.

Keywords Argonaute · Mg^{2+} · MiRNA-mRNA · MM/GBSA · Molecular dynamic simulation

Electronic supplementary material The online version of this article (doi:10.1007/s00894-012-1377-4) contains supplementary material, which is available to authorized users.

Z. Ma · H. Zhang · Y. Wang
Center of Bioinformatics, Northwest A&F University,
Yangling 712100, Shaanxi, China

Z. Ma · H. Zhang · Y. Wang (✉)
College of Life Sciences, Northwest A&F University,
Yangling 712100, Shaanxi, China
e-mail: yh_wang@nwsuaf.edu.cn

Z. Xue
Computer Network Information Center,
Chinese Academy of Sciences,
Beijing 100190, China

Y. Li
School of Chemical Engineering,
Dalian University of Technology,
Dalian 116012, Liaoning, China

Introduction

MicroRNAs (miRNAs), approximately 19–23 nucleotides, are categorized as a family of non-protein-coding, endogenous small RNAs, playing critical roles in many biological processes, such as apoptosis, the metabolism pathways and even brain development [1, 2]. Since the first miRNA was reported in the early 1990s [3], the interest in miRNAs has increased tremendously in order to get more insights into the RNA interference world. So far, several-thousands of miRNAs have been isolated from many organisms by using a set of ingenious molecular methods [2]. Intensive research involving miRNA participation in various physiological processes have been performed [4, 5]. More recently, lots of related studies were conducted in our lab. For instance, in systems biology, we have examined and quantified the dynamic properties, key rate-limiting steps as well as the stochastic noise that underlies the generic miRNA pathway [6, 7], and in the molecular dynamic studies, we have characterized the molecular mechanisms of Exportin-5 recognizing

and transporting the pre-miRNA [8] and the molecular basis of miRNA interacting with the Ago protein and its target, which have uncovered the key elements required for recognition of the miRNA target [9].

MiRNA functions its-targeted RNA cleavage, which is mediated by the RNA induced silencing complex (RISC) containing Dicer, TRBP and argonaute (Ago) proteins [4]. The RISC complex with the guide strand of miRNA recognizes the complementary messenger RNA (mRNA) molecules and degrades them or inhibits their translation, leading to the substantially decreased levels of protein translation and effectively turning off the gene. As the catalytic components of RISC [10], Ago protein has two distinguishing domains, i.e., the PAZ and PIWI domains; the former is found in Dicer family proteins whereas the latter is restricted to Argonautes [11]. The PAZ domain consists of two subdomains, the first subdomain is composed of a five stranded open β -barrel with two helices on one end of the barrel, and the second is made up of a β -hairpin followed by an α -helix [12]. The conserved aromatic residues of the PAZ domain form a deviant oligonucleotide fold containing a central cleft that allows Ago to bind the single-strand 3' end of the small RNA in RISC specifically [13–15]. The PIWI domain sits at the center of the crescent-shape Ago and extends to the protein C-terminus. The PIWI core fold is similar to the RNase H enzyme with conserved active aspartates, implicating that Ago has the RNA cleavage or 'slicer' activity [16, 17]. A recent report showed that RISC is an Mg^{2+} -dependent endonuclease in both humans and flies [18], which was also evidenced by the crystal structure of Ago complex. Structurally, three structural Mg^{2+} cations were found in the complex, with one cation (Mg1) bound to Q414 embedded in the Mid domain which might be involved in the anchoring of 5' end phosphate of miRNA, and one cation (Mg2) bound to D459, A460, and D635, yet the third cation (Mg3) coordinated by the catalytic triad (D459, E490 and D524) of the RNase H fold of the PIWI domain, the catalytic site for mRNA cleavage (Fig. 1).

The cognate target mRNA is cleaved by the RISC complex with the aid of Mg^{2+} , which catalyze the hydrolysis of mRNA and stabilize the reaction transition state meanwhile [18]. Our recent work also demonstrated that Mg1 plays an important role in the recognition process of miRNA by Ago, and Mg2 and Mg3 are the key factor in producing and stabilizing the geometry of the catalytic triad [9]. As a matter of fact, Mg^{2+} ion is critical for the structure and properties of many macromolecules [19]. For instance, in transporter *mgtA* gene, Mg^{2+} modifies the structure of *mgtA* 5'UTR with different concentrations [20]. Additionally, Mg^{2+} is involved in protein correct folding [21], structural stability [22], and catalytic activity [23]. For example, in the hammerhead ribozyme, one Mg^{2+} ion is observed to bind to

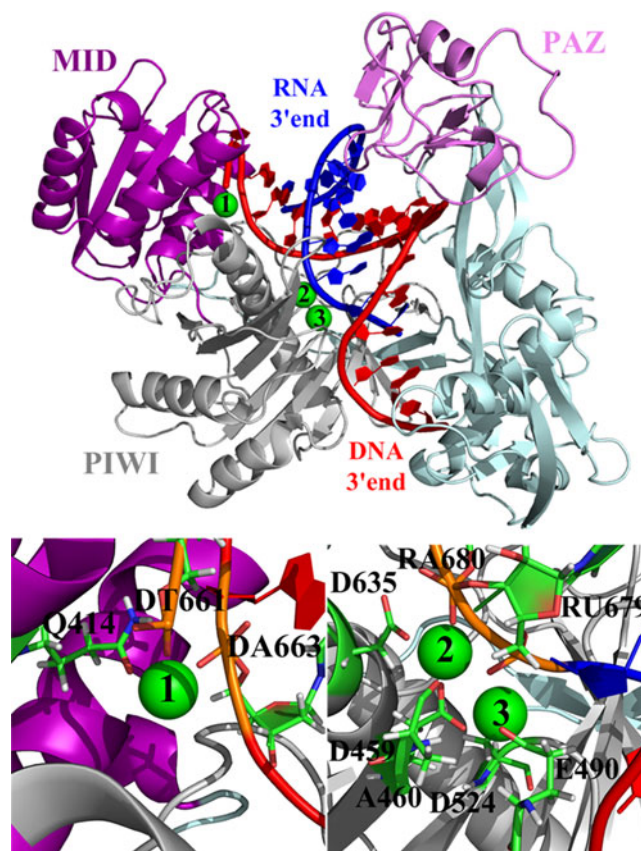


Fig. 1 Cartoon of the Ago-DNA complex. The Ago protein is color-coded by domains (N in pale cyan, PAZ in violet, Mid in purple and PIWI in gray); The guide DNA is in red and whereas the target RNA is in blue; The Mg^{2+} (green) molecules are shown as spheres, Mg1, Mg2 and Mg3 are marked 1, 2 and 3; The residues Q414 and the base DT661, DA663 bound to Mg1, the residues D459, A460, D635 and the base RU679, RA680 bound to Mg2, the residues D459, E490, D524 and the base RU679 bound to Mg3 are colored by element

the ribozyme and facilitates the formation of near in-line attack conformations [24].

However, how these cations affect the systematic dynamics of a complex, particularly for the RISC, still remains unclear, experimental observation for the conformational changes of a protein is very hard to perform due to the impact of metal cations. In order to investigate the influence of Mg^{2+} on miRNA-target interactions, 16 systems in absence/presence of different Mg^{2+} were investigated in this work by molecular dynamics simulation and thermodynamic analysis with molecular mechanics generalized Born surface area (MM-GBSA) method.

Materials and methods

As RNA always tends to decay in situ, it is difficult to determine the 3D structure of Ago-RNA complex, much less

the structure of Ago-miRNA-mRNA complex. Therefore, in this work, the 3.0 Å crystal structure of wild-type *T. thermophilus* Ago complexed with a 5'-phosphorylated guide DNA and its complementary target RNA (PDB entry 3HVR [5]), were used to generate the initial protein coordinates for the MD simulations. The side chains with missing coordinates were reconstructed by using the package of Deepview [25]. The DNA sequence is GAGGTAGTAGTTGT, with the seed segments underlined, the target RNA seed sequence is CUCCAUC from the 5'-end of the guide strand. Three Mg²⁺ cations were found in the crystal structure: the first cation (Mg1) coordinated by Q414 embedded in the Mid domain which might be involved in the anchoring of 5' end phosphate of miRNA, the second cation (Mg2) bound to the catalytic triad (D459, D524 and D635) of the RNase H fold of the PIWI domain, the catalytic site for mRNA cleavage, yet the third one (Mg3) which resides in the neighboring of Mg2 with distance of ~4.4 Å is also located at PIWI domain surrounded by D459, E490 and D524 as shown in Fig. 1.

It is speculated that Mg²⁺ ion might bind to the RNA substrate through a nonbridging oxygen of the scissile phosphate during catalysis, however, the detailed mechanism concerning the presence of different Mg²⁺ function in the process of RISC mediated target RNA recognition still remains unknown, to solve this query 16 simulation systems are performed in this work. The crystal structure is modified to meet our need by removing DNA-RNA or Mg²⁺ by using pymol software [26], and the initial coordinates of 16 systems are obtained. The systems free Ago (P₀), Ago-Mg1 (P₁), Ago-DNA-RNA (C₀) and Ago-DNA-RNA-Mg1 (C₁) are created to explain the function of Mg1; Ago-Mg2 (P₂) and Ago-DNA-RNA-Mg2 (C₂) are added to get more information about Mg2 function; while, the systems Ago-Mg3 (P₃), Ago-DNA-RNA-Mg3 (C₃) are also taken in account to interpret how Mg3 works during the RNAi pathway and Ago-Mg1-Mg2 (P₁₂), Ago-Mg1-Mg2-Mg3 (P₁₂₃), Ago-DNA-RNA-Mg1-Mg2 (C₁₂), Ago-DNA-RNA-Mg1-Mg2-Mg3 (C₁₂₃), Ago-Mg1-Mg3 (P₁₃), Ago-DNA-RNA-Mg1-Mg3 (C₁₃), Ago-Mg2-Mg3 (P₂₃), Ago-DNA-RNA-Mg2-Mg3 (C₂₃) are carried out to explore the interaction between these ions.

MD simulations

All molecular dynamics simulations were carried out using the GROMACS 4.0 package [27] with the AMBER99 forcefield [28]. For MD simulations, 16 models (free Ago, Ago-Mg1, Ago-Mg2, Ago-Mg3, Ago-Mg1-Mg2, Ago-Mg1-Mg3, Ago-Mg2-Mg3, Ago-Mg1-Mg2-Mg3, Ago-DNA-RNA, Ago-DNA-RNA-Mg1, Ago-DNA-RNA-Mg2, Ago-DNA-RNA-Mg3, Ago-DNA-RNA-Mg1-Mg2, Ago-DNA-RNA-Mg1-Mg3, Ago-DNA-RNA-Mg2-Mg3 and

Ago-DNA-RNA-Mg1-Mg2-Mg3) were solvated with the TIP3P water model [29] and 85Na⁺ 105Cl⁻, 85Na⁺ 107Cl⁻, 85Na⁺ 107Cl⁻, 85Na⁺ 107Cl⁻, 85Na⁺ 109Cl⁻, 85Na⁺ 109Cl⁻, 85Na⁺ 109Cl⁻, 85Na⁺ 111Cl⁻, 93Na⁺ 85Cl⁻, 91Na⁺ 85Cl⁻, 91Na⁺ 85Cl⁻, 91Na⁺ 85Cl⁻, 89Na⁺ 85Cl⁻, 89Na⁺ 85Cl⁻, 89Na⁺ 85Cl⁻, 89Na⁺ 85Cl⁻, 87Na⁺ 85Cl⁻ were added to neutralize the total charge and bring the ionic strength of the solvent to physiological levels of 0.15 M, respectively. The V-rescale thermostat [30] was applied using a coupling time of 0.1 ps to maintain the systems at a constant temperature of 300K, with pressure maintained by coupling to a reference pressure of 1 bar, and values of the isothermal compressibility set to $4.5 \times 10^{-5} \text{ bar}^{-1}$ for water simulations. Periodic boundary conditions were employed and particle mesh Ewald [31] was used for the long-range electrostatic interactions. Van der Waals and Coulomb interactions were truncated at 1.4 and 1.0 nm, respectively. All bond lengths including hydrogen atoms were constrained by the LINCS algorithm [32]. For each system, the simulation cell was a rectangular box, with the size of 108.51 Å × 98.77 Å × 87.77 Å, and the minimum distance between the protein and the box wall was set to be larger than 10 Å, so that the protein does not interact with its own periodic images via truncated van der Waals interaction (Lennard-Jones potential) and the long range electrostatic interactions with this image are sufficiently small. Numerical integration of the equations of motion used a time step of 2 fs, with non-bonded pair list updated every 10 steps and conformations stored every 2 ps for analysis.

After initial configuration construction, a standard equilibration protocol was performed for molecular simulations. The system was subjected to energy minimization for 10,000 steps by steepest descent and for 15,000 steps by conjugate gradient to avoid close atomic contacts, followed by slow constant volume heating to 300 K over 100 ps using $2.4 \text{ kcal mol}^{-1} \text{ Å}^{-2}$ harmonic restraints. These restraints were slowly reduced to zero during a series of energy minimizations and 100 ps equilibration steps at constant temperature (300 K) and pressure (1 bar) with a 0.2 ps coupling constant for both parameters. The final equilibration step was a 200 ps constant volume run under NPT (constant pressure and constant temperature) conditions. The production stage consisted of a total of 25 ns at constant temperature of 300 K and constant pressure of 1 bar (NPT ensemble) for all the 16 systems, respectively.

Cross-correlation analyses

The dynamic characteristics of the protein in the simulations can be analyzed to yield information about correlated motions [33]. The motions of the proximal residues can be calculated by cross-correlation and also between regions as

in domain–domain communication. The degree of collective motions between different groups of atoms was assessed from the cross-correlation matrix with elements

$$Corr_{ij} = \frac{\langle (\vec{r}_i - \langle \vec{r}_i \rangle) \cdot (\vec{r}_j - \langle \vec{r}_j \rangle) \rangle}{\langle (\vec{r}_i - \langle \vec{r}_i \rangle)^2 \rangle^{\frac{1}{2}} \cdot \langle (\vec{r}_j - \langle \vec{r}_j \rangle)^2 \rangle^{\frac{1}{2}}} \quad (1)$$

Each element represents the correlation of the movements of atoms *i* and *j*. The three-dimensional dynamical cross-correlation map (DCCM) [34] displays the elements $Corr_{ij}$, which can be collected in matrix form. In the present study, the correlated motion of a residue pair is represented by the motion of the C α atoms of those residues from 10 ns to 25 ns of the MD trajectory. In the case of positively correlated residues move in the same direction, $Corr_{ij}$ equals 1, whereas negative residues move in the opposite direction, it is -1 , while noncorrelated or perpendicular, it is 0.

Binding free energy calculation

Molecular mechanics generalized Born surface area (MM-GBSA) [35] a continuum solvent approach and approximates the “average” free energy of a state to calculate binding free energies, and all of these are based on an analysis of molecular dynamics trajectories. Based on the MM-GBSA method integrated in AMBER 10 [36], the binding free energy ΔG of each system could be conceptually described as follows:

$$\Delta G = \Delta E_{MM} + \Delta G_{SOL} - T\Delta S_{MM} \quad (2)$$

where ΔG (Eq. 2) is the binding free energy in solution, ΔE_{MM} corresponds to the molecular mechanics energy, or enthalpic, contribution and is given by:

$$\Delta E_{MM} = \Delta E_{bond} + \Delta E_{angle} + \Delta E_{torsion} + \Delta E_{vdw} + \Delta E_{ele} \quad (3)$$

$$\Delta G_{SOL} = \Delta G_{SA} + \Delta G_{GB} \quad (4)$$

$$\Delta G_{SA} = \gamma SA + \beta \quad (5)$$

ΔG_{SOL} , the solvation energy belonging to enthalpic contribution, is given by two parts. First, there is the nonpolar contribution ΔG_{SA} (Eq. 5), that contains the product of the surface area and an effective surface tension term. However, the further corrections based on attractive and repulsive solvent–solute interactions that improve the estimate of the nonpolar contribution [37]. This part of the solvation free energy was estimated by using a linear scaling factor of $\gamma=0.0072$ kcal/(mol/Å²) and $\beta=0.00$ kcal mol⁻¹, derived

from Eq. 5 and SA is the solvent accessible surface area calculated from the program MSMS [38]. Second, the electrostatic contributions to the solvation energy are modeled by the generalized Born model [39]:

$$\Delta G_{GB} = -\frac{1}{2} \left(1 - \frac{\exp(-kF_{GB})}{\epsilon_\omega} \right) \sum_{lm} \frac{Q_l Q_m}{F_{GB}} \quad (6)$$

ϵ_ω is the solvent dielectric constant, Q_l and Q_m are atomic partial charges, k is the Debye–Hückel screening parameter. A smooth function that depends on atomic radii and the distance between two atoms is defined as:

$$F_{GB} = \left[r_{lm}^2 + \alpha_l \alpha_m \exp\left(\frac{-r_{lm}^2}{4\alpha_l \alpha_m}\right) \right]^{\frac{1}{2}} \quad (7)$$

r_{lm} is the distance between atom *l* and *m*, α_l and α_m are the effective Born radius of atom *l* and *m*. The dielectric constants of 1 and 80 were used for the interior and exterior of the solute, respectively. The dielectric boundary was defined using a 1.4 Å probe on the atomic surface. The entropy term $T\Delta S_{MM}$ (Eq. 2) which was estimated by normal-mode analysis using the nmode module in AMBER 10, is the contribution of conformational entropy to the binding free energy.

The total binding free energy of the ligand-receptor interaction was decomposed into the contribution from each individual residue by using the MM-GBSA method. The decomposed binding free energy of ligand-receptor residue pair includes three terms (the entropy term is neglected because of its inaccurate estimation and costly time/memory requirements): electrostatic contribution (ΔE_{elec}), van der Waals contribution (ΔE_{vdw}) and solvation contribution ($\Delta E_{solvation}$). The contribution of atom *l* to the electrostatic free energy of binding is obtained by formula (8):

$$e_{elec}^l = -\frac{1}{2} \sum_m \left(1 - \frac{\exp(-kF_{GB})}{\epsilon_\omega} \right) \frac{Q_l Q_m}{F_{lm}^{GB}(r_{lm})} + \frac{1}{2} \sum_{l \neq m} \frac{Q_l Q_m}{r_{lm}} \quad (8)$$

Because the internal energy contribution arising from bond, angle and dihedral terms ΔE_{int} is equal to zero, the calculation of internal energies have been canceled. A recursive algorithm was used to estimate the SASA [40] and the corresponding SASA determined the corresponding non-polar solvation energy of each atom. Moreover, e_{elec}^l includes one half of the ligand-receptor pair van der Waals interaction energy. By summing the relative contribution of each atom of a given residue, the total binding free energy of the residue can be obtained. The relevant atoms are also organize the separate contribution of backbones and side-chains. Finally, all energy components were calculated by

using a total of 100 snapshots that were extracted from the simulation trajectory.

Results and discussion

Protein structure and dynamics

Figure 2 shows the root-mean-square deviation (RMSD) values of the conformational drift of Ago protein of $C\alpha$ atoms respect to the starting structures. In general, the trajectories remain stable with average RMSD values of about 4–7 Å for the single Ago systems and 2–5 Å for the DNA-RNA bound ones. Meanwhile, it is observed that the presence of different Mg^{2+} influences the degree of conformational drift of the Ago protein.

For the P_0 and C_0 systems, after a rise in the first 10 ns, the overall $C\alpha$ RMSD reach stable plateaus with RMSD of 5.53 ± 0.96 Å and 2.60 ± 0.36 Å respectively. However, after the binding of Mg1, the P_1 and C_1 systems show a larger fluctuation with RMSD of 5.75 ± 1.1 Å and 3.62 ± 0.70 Å, indicating that Mg1 increases the fluctuation of the protein structure.

Interestingly, we observe that the binding of Mg2 to the Ago protein shows a more complex dynamics behavior than that of Mg1. Without bound DNA-RNA, both the P_0 and P_2 systems show similar fluctuation (5.53 ± 0.96 Å for the former and 4.82 ± 1.1 Å for the later). While after the binding of DNA-RNA, the motion of Ago in the C_2 (RMSD= 4.16 ± 0.80 Å) system is much larger than that in the C_0 (RMSD=

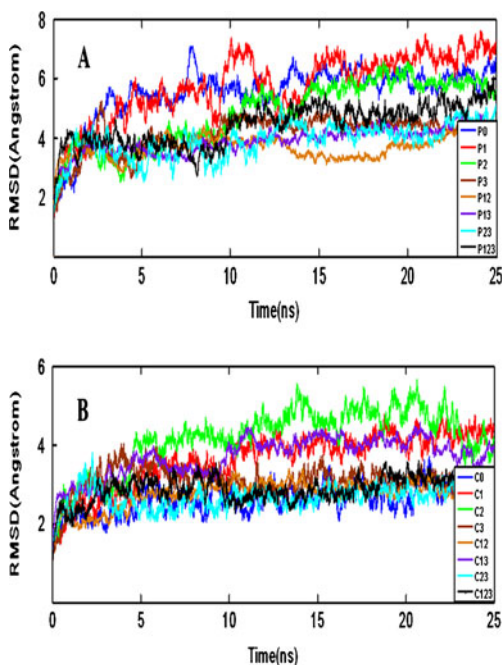


Fig. 2 The root-mean-square deviations (RMSD) of the $C\alpha$ atoms relative to their starting structures as a function of time: **a** for Ago without DNA-RNA; **b** for Ago with DNA-RNA

2.60 ± 0.36 Å) system. The combined results imply that the cooperation of Mg2 and DNA-RNA have effects on the conformational change of the Ago protein.

In contrast to the influence of Mg1 on the Ago protein, the binding of Mg3 inhibits the movement of the protein, which is supported by the much lower RMSD (4.14 ± 0.62 Å) in the P_3 system compared with the P_0 (RMSD= 5.53 ± 0.96 Å) system. Similarly for the C_{23} and C_2 systems, the Ago protein exhibits a significantly decreased fluctuation (~ 2 Å) with the binding of Mg3 with the RMSD value of 4.09 ± 0.83 Å, indicating that the presence of a bound Mg3 actually stabilizes the conformation of Ago.

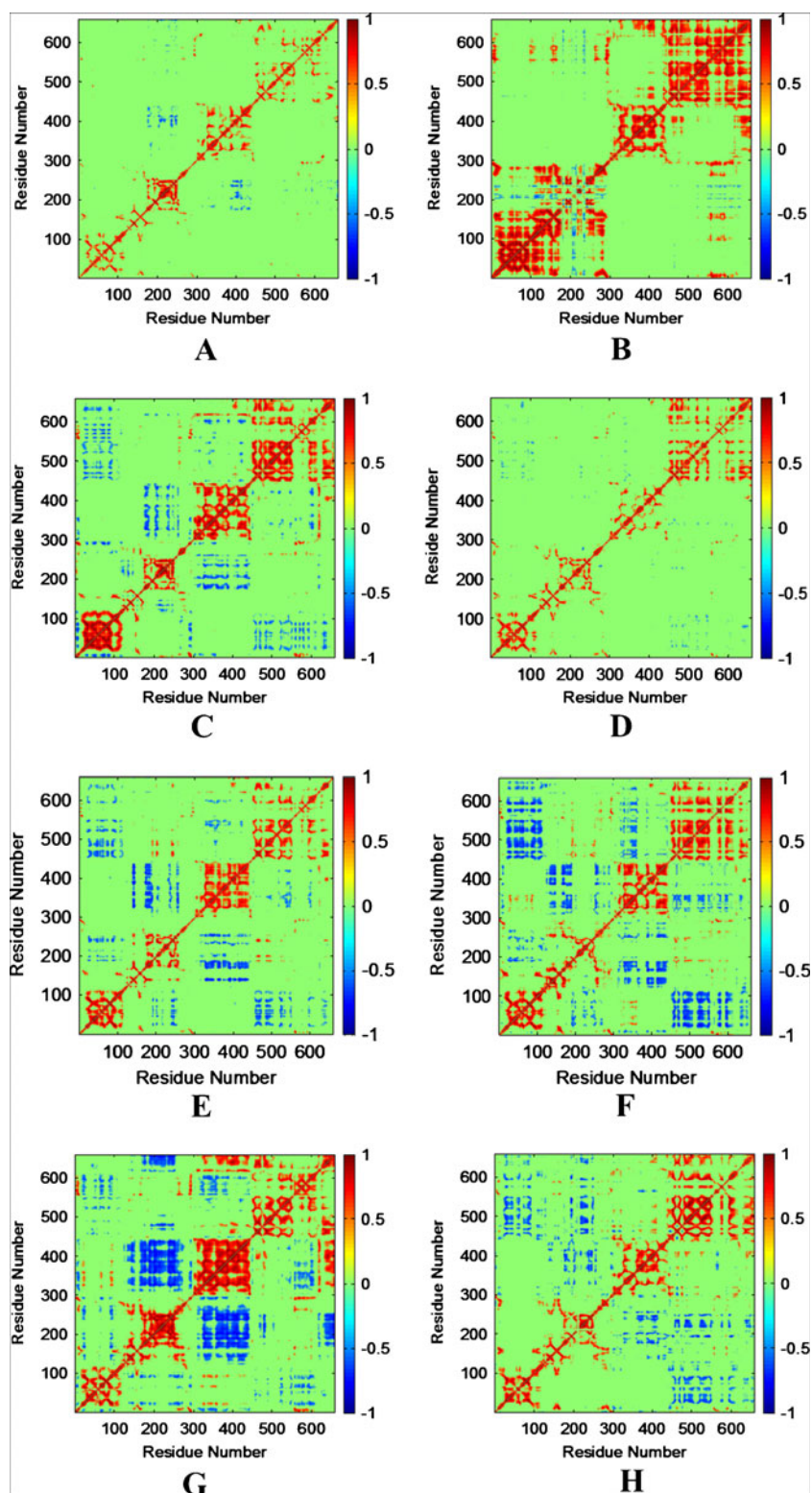
The above analysis indicates that Mg1, Mg2 and Mg3 exhibit different binding properties at certain locations of the Ago protein, and probably have divergent functions, although the exact nature of this difference is not clear based on the RMSD analysis. In order to solve this, the dynamical cross-correlation matrix of residues was further performed.

Cross-correlation analysis

Figures 3 and 4 exhibit the dynamical cross-correlation maps of the 16 simulations. For each system, the last 17 ns simulated trajectories are used to construct the dynamical cross-correlation matrix. The absolute value of correlation coefficients above 0.5 is reported for each dynamical cross-correlation map, which acts as a threshold to capture correlations of the domains of Ago. In the present work, positive or in-phase correlations are colored in red (strong), while negative or out-of-phase correlations are colored in blue (strong).

First, we compare the cross correlation maps of the P_0 and P_1 systems in order to investigate the influence of Mg1 on the pattern of Ago movement. Figure 3a and b show that the average correlation coefficient (R) of Mid domain (residue 316–445) in the free Ago system is relatively lower ($R=0.38$) than that in the Mg1 bound system ($R=0.69$), indicating that Mg1, embedded in the Mid domain, stabilizes the correlated motion of the Mid domain to some extent. Consistent with the influence of Mg1 in the Mid domain, we find that the correlated motions of N-terminal (residue 12–170), PIWI domain (residue 446–660) increase by 0.73, 0.63 after the binding of Mg1 (Fig. 3b), revealing that Mg1 can increase the in-phase motion of the two domains, which is in agreement with the previous RMSD result. Interestingly, we also observe negative correlations between PAZ (residues 176–256) and N-terminal, PIWI domains, which represent the out-of-phase movements between these domains (Fig. 3b). And the presence of Mg1 increases the anticorrelated motion ($R=-0.55, -0.56$) between PAZ and N-terminal, PIWI domains, implying that the binding of Mg1 enlarges the movements of PAZ/N-terminal cleft and the PAZ/PIWI cleft, and thus favors the insertion of DNA-RNA and let the first ($5'$) and third phosphates of the DNA guide strand coordinate to Mg1 readily [41]. However, a cross

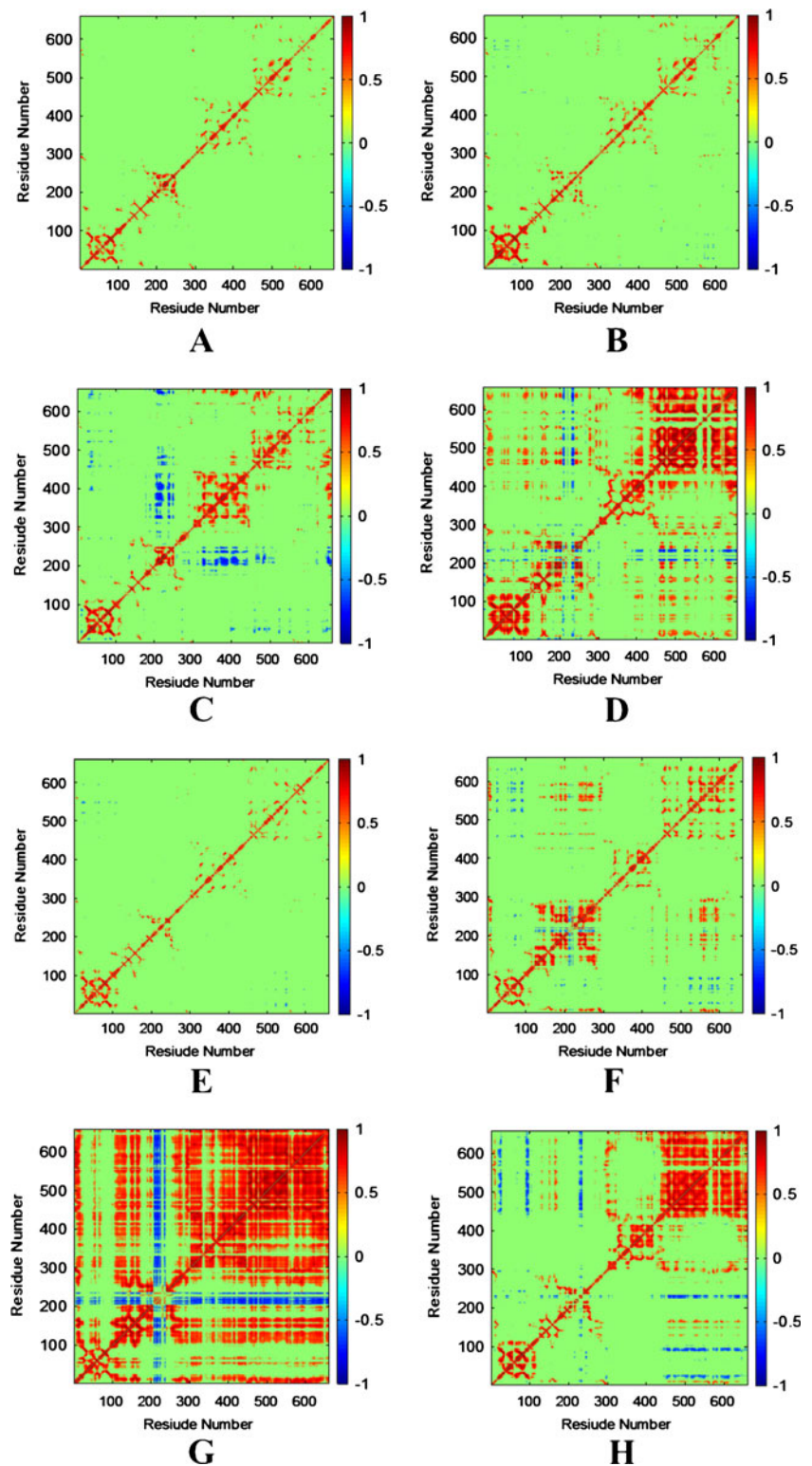
Fig. 3 Dynamical cross-correlation maps illustrating the correlation of motion between residues in (a) free Ago (P_0), (b) Ago-Mg1 (P_1), (c) Ago-Mg2 (P_2), (d) Ago-Mg3 (P_3), (e) Ago-Mg1-Mg2 (P_{12}) (f) Ago-Mg1-Mg3 (P_{13}), (g) Ago-Mg2-Mg3 (P_{23}), (h) Ago-Mg1-Mg2-Mg3 (P_{123})



correlation comparison between the C_0 and C_1 systems shows that the presence of Mg1 does not have an effect on the fluctuation of Ago protein (Fig. 4a and b). The reason lies in the formed hydrogen bonds between DNA-RNA and the protein [42], which fix these domains to a certain extent.

Subsequently, we contrast the cross correlation maps of P_0 system and P_2 system to gain more information about the effect of Mg2 on the movement of the Ago protein. Figure 3c shows that the anticorrelated motion between the N-terminal and the PIWI domains, and between the

Fig. 4 Dynamical cross-correlation maps illustrating the correlation of motion between residues in (a) Ago-DNA-RNA (C_0), (b) Ago-DNA-RNA-Mg1 (C_1), (c) Ago-DNA-RNA-Mg2 (C_2), (d) Ago-DNA-RNA-Mg3 (C_3), (e) Ago-DNA-RNA-Mg1-Mg2 (C_{12}), (f) Ago-DNA-RNA-Mg1-Mg3 (C_{13}), (g) Ago-DNA-RNA-Mg2-Mg3 (C_{23}), (h) Ago-DNA-RNA-Mg1-Mg2-Mg3 (C_{123})



PAZ and the Mid domains is increased in the presence of Mg2, as evidenced by the increased average correlation coefficient ($R=-0.53$ for the former, and $R=-0.58$ for the later), indicating that Mg2 can significantly increase the fluctuation of these domains. This result implies that the

presence of Mg2 increases the anticorrelated motion between adjacent regions, therefore resulting in a strong “open-close” motion which is more convenient for the binding of DNA-RNA. In addition, comparison between the C_0 and C_2 systems further shows that the binding of Mg2 also

enhances the anti-movements between the PAZ (residue 200–240) and the MID (residue 310–430) domains, as evidenced by the increased fluctuation in the C₂ system (Fig. 4c) ($R=-0.54$) compared to the system C₀ (Fig. 4a) ($R=-0.51$). This suggests that the presence of Mg²⁺ enhances the out-of-phase motion between the PAZ region and the MID and PIWI regions, which probably favors the separation of RNA from the Ago protein, i.e., the degradation of this nucleic acid chain [43].

In contrast to the effects of Mg¹ and Mg² on the protein, the cross correlation map of P₃ system (Fig. 3d) shows a lower degree of correlated/anticorrelated motion of the Ago protein after the binding of Mg³ compared with the P₀ system (Fig. 3a), especially in the PAZ and Mid domains. This indicates the presence of Mg³ can reduce the movement of these domains, in line with our RMSD results (5.53 ± 0.96 Å for the P₀ system, and 4.14 ± 0.62 Å for the P₃ system). Interestingly, the much larger size of red patch in the C₃ system (Fig. 4d) shows significantly increased positive correlation of the N-terminal, Mid and PIWI domains, compared with the C₀ system (Fig. 4a). The observation is reminiscent of that combined with DNA-RNA; Mg³ enables to increase the correlated motion of these domains, which is induced by the hydrogen bonds between the DNA-RNA and the protein.

The interactions among Mg²⁺, local water and residues

Water plays a vital role in determining the structures and dynamics of proteins, the dynamic behavior of water on the protein surface reveals significant features about the stability and the potential interactions of the protein [44]. For metal ions required for the proper function of all cells within living organism, magnesium, as the critical divalent intracellular cation, is essential for a variety of cellular processes such as enzyme function, DNA and protein synthesis, and the regulation of ion channels [45]. Moreover, the polarizability of ions and water molecules can affect the hydration structure and dynamics of the local regions [46]. This raises some questions whether the water affects the ion binding to the protein; what roles of the Mg²⁺ and the hydration water play in the local regions; how the conformations of the local residues change on the structure and stability of the Ago under the effects of the Mg²⁺ and the hydration effects? In the present work, to address these questions, the atom coordinates are transformed by superimposing every snapshot onto the average structure in all the simulation systems, and then several highly occupied hydration sites, which are high density regions in the three dimensional time averaged solvent structure in molecular dynamics simulations and diffraction experiments, are revealed around the Mg²⁺ binding sites (Figs. 5 and 6) and the analysis of the Mg²⁺ and the hydration effects on the local regions of the Mg²⁺ binding sites are carried out on all the simulation systems.

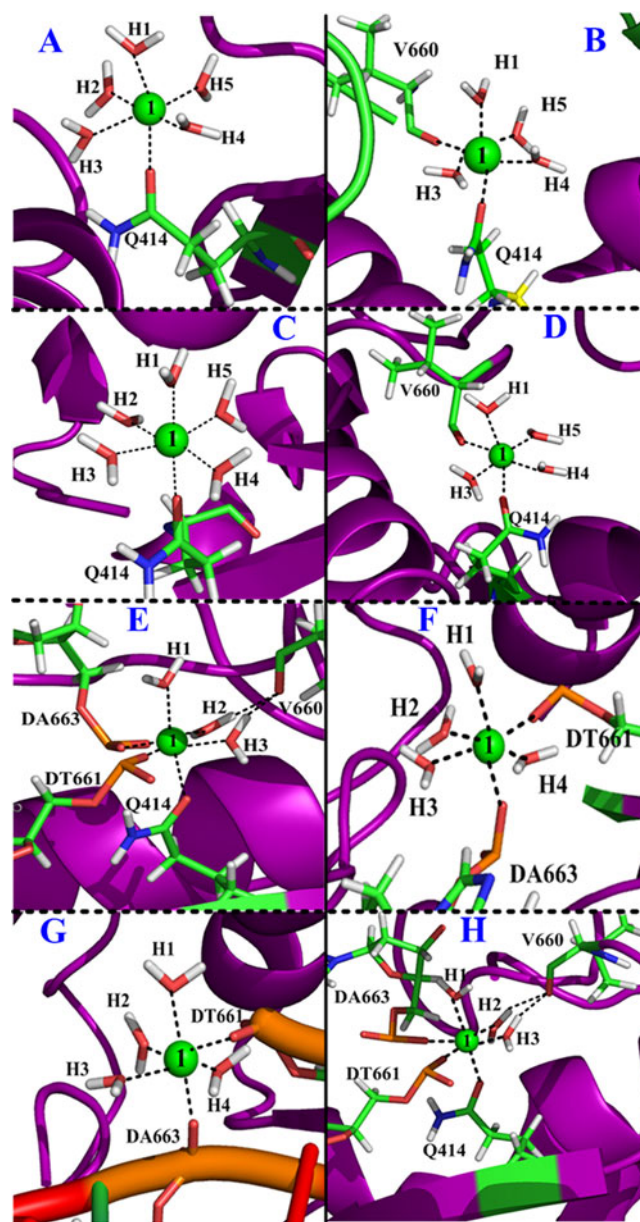


Fig. 5 Equilibrated coordination of the magnesium ion (Mg¹) binding site. The water distribution of Mg¹ binding site and the geometry of octahedron formed by the surrounding water and the involved residues. **a** for P₁ system, **b** for P₁₂ system, **c** for P₁₃ system, **d** for P₁₂₃ system, **e** for C₁ system, **f** for C₁₂ system, **g** for C₁₃ system and **h** for C₁₂₃ system. The hydration water H₁, H₂, H₃, H₄, H₅ stay stable, all other water molecules do not stay constant in this region

Mg¹ and the local hydration effects

The free Ago, Ago-Mg¹, Ago-DNA-RNA and Ago-DNA-RNA-Mg¹ trajectories under scrutiny show: water molecules surrounding the Mg¹ binding region in the P₀ system (Fig. 7a) are sporadic as there is no constraint force to make the water molecules reside a long time, leading to a larger fluctuation for local residues Q414 and V660 as evidenced by the average

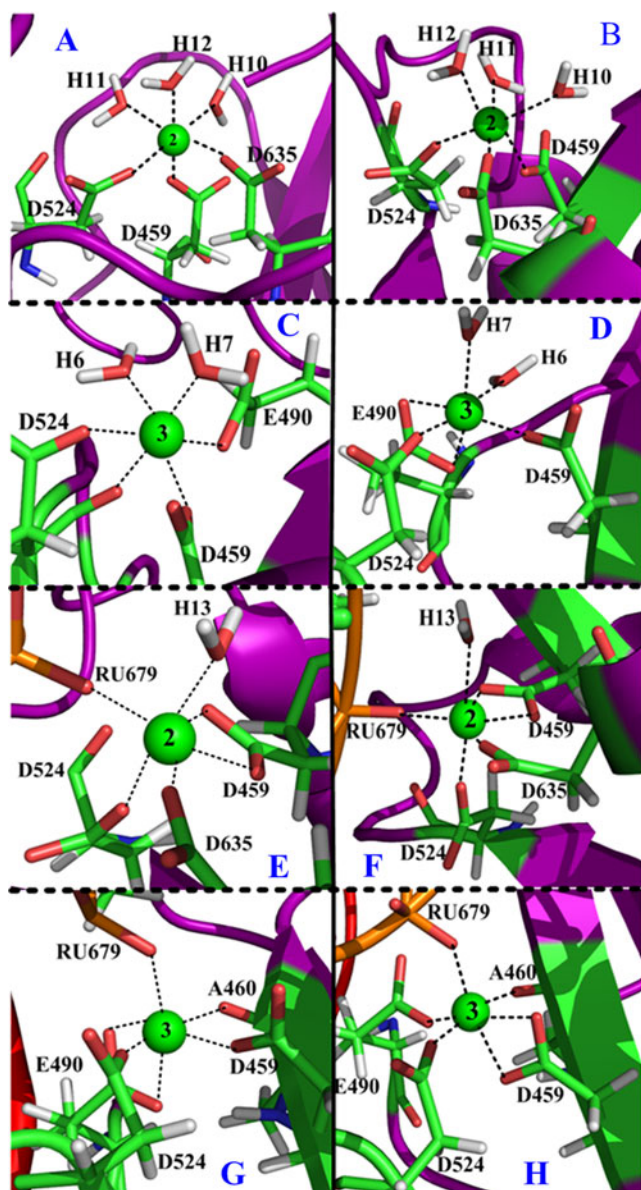


Fig. 6 Equilibrated coordination of the magnesium ions binding site Mg2 and Mg3. The water distribution of Mg2 and Mg3 binding sites and the geometry of octahedron formed by the surrounding water molecules and the involved residues. **a** for P₁₂ system, **b** for P₂ system, **c** for C₁₃ system, **d** for C₃ system, **e** for C₁₂ system, **f** for C₂ system, **g** for C₁₃ system and **h** for C₃ system. The hydration water H6, H7, H8, H9, H10, H11, H12, H13 stay stable, all other water molecules do not stay constant in this region

RMSD of ~1.2 Å. While for the P₁ system (Fig. 5a), we observe that five hydration sites (H1, H2, H3, H4 and H5) are produced with residence time over 22 ns (the high occupancy of 90% during the whole simulation) and these hydration sites form an octahedron arrangement with Mg1 and Q414 (the distances between Mg1 and Q414, hydration water molecules are approximate to 2 Å). This result indicates that the binding of Mg1 makes interaction with Q414 and stabilizes the local region of Ago protein as evidenced by an average RMSD less

than 1.0 Å. Notably, the transition from the Ago-Mg1 system to the Ago-DNA-RNA-Mg1 system does not cause switches of H1, H2 and H3 but results in the vanishing of H4 and H5, which are substituted by the bases (DT661 and DA663) of the guide DNA (Fig. 5e). This result shows that Mg1, located at the interface between Ago and DNA-RNA, interacts with water in the five hydration sites to act as the extended side chains of Ago with the purpose of capturing DNA-RNA, suggesting that the presence of Mg1 and its surrounding hydration water molecules is favorable to the insertion of DNA-RNA.

Mg2 and the local hydration effects

In P₂ system, Mg2 is well located at the center of octahedron by interacting with water molecules at three hydration sites (H10,

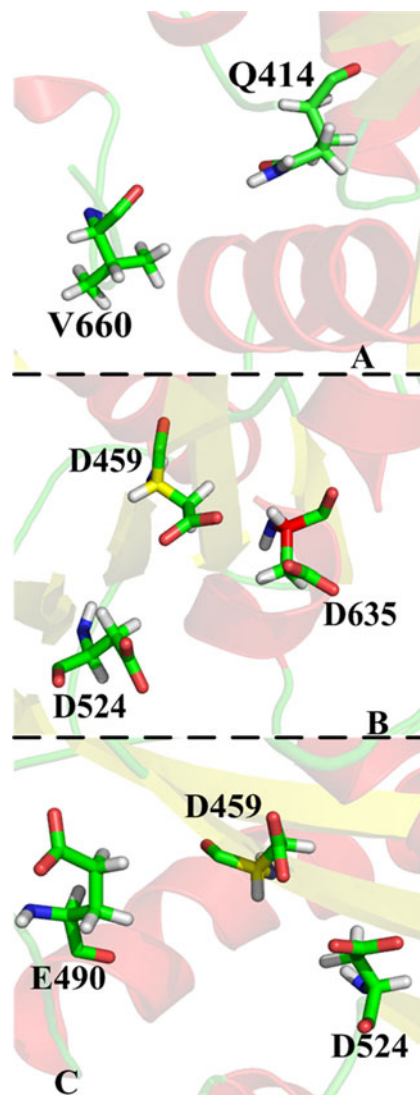


Fig. 7 The conformation of the local residues of the magnesium ions binding site in an equilibrated coordination, **a** for Mg1 binding site, **b** for Mg2 binding site and **c** for Mg3 binding site

H11 and H12) with a long residence time over 22 ns (the high occupancy of 90% during the whole simulation) (Fig. 6b). Meanwhile, this ion interacts with the carboxyl groups of D459, D524 and D635, which form a conserved DDD motif required for the cleavage [47]. This result implies that the Mg²⁺-coordinated DDD motif of the PIWI domain might cleave the target RNA by the presence of Mg²⁺ in C₂ system, favoring the separation of RNA from the Ago protein by enhancing the out-of-phase motion between the PAZ region and the MID and PIWI regions, which is revealed by more deep blue color of the PAZ, MID and PIWI domains (usually indicates more fluctuation) in C₂ system than C₀ system in the cross-correlation maps. However, the residues (D459, D524 and D635) in P₀ system are quite dispersed as evidenced by the long distances between them, which are ~5.76 Å (D459-D524, ~3.84 Å in P₂), ~7.67 Å (D524-D635, ~4.62 Å in P₂), ~4.90 Å (D459-D635, ~4.49 Å in P₂) and the geometry of the local region becomes irregular (Fig. 7b). The observation for another side reveals that the binding of Mg²⁺ can facilitate to form the regular geometry for the involved residues with Mg²⁺ (Fig. 6b). While after the binding of DNA-RNA (Fig. 6f), the number of the hydration sites is decreased to one, showing that the bases of RNA (RU679 and RA680) replace two hydration sites to coordinate with Mg²⁺. The long-residing (over 22 ns) and tightly bound water molecules (Table S1) in the octahedral arrangement are functionally significant, facilitating the RNA hydrolysis during catalytic cleavage by RNase-H-containing nucleases together with the Mg²⁺ cation [48].

Mg3 and the local hydration effects

In P₃ system, we only observed two hydration sites surrounding Mg²⁺ (Fig. 6d), and the oxygen atoms of water molecules in the hydration sites combined with the other four oxygen atoms of D459, E490 and D524 to form an octahedral arrangement. Mg²⁺ is well located at the center of the arrangement and forms stable interactions with the oxygen atoms of the amino acids in Ago with the distance of ~2 Å (Table S1). In addition, the patterns for how Mg²⁺ affects the local conformation shown in “Mg²⁺ and the local hydration effects” section is also obtained for the Mg²⁺ binding region (Fig. 7c), which also demonstrates that Mg²⁺ provides a strong polarization effect on the surrounding residues and water (RMSD of ~0.6 Å) (Fig. S1) to form a stable structure. Strikingly, after the binding of DNA-RNA, all of the hydration sites disappear (Fig. 6h), base RU679 and residues D459, A460 and E490 form stable bonds with Mg²⁺ (~2 Å) instead. In this RNA binding process, Mg²⁺ might act as a “guide” who firstly builds a well arranged water hydration network and in this way leads RNA to bind to Ago protein correctly. This is in agreement with the previous study that binding partnerships enable to help the Ago protein to interact with DNA-RNA.

Interactions between Mg1 and Mg2, Mg3

The above analysis implies that Mg²⁺, Mg²⁺ and Mg²⁺ show divergent functions and different binding properties at Ago, while it is still unclear how Mg²⁺ and Mg²⁺ affect the local conformation of Mg²⁺ neighborhood. To gain the insight into this question, we further analyze the interaction among these Mg²⁺ ions. First, we compare the P₁ system (Fig. 5a) with the P₁₂₃ system (Fig. 5d) to investigate the effect of the presence of Mg²⁺-Mg²⁺ on the Mg²⁺-coordination geometry. The comparison study shows that the local geometry of Mg²⁺ is changed after the binding of Mg²⁺-Mg²⁺: the number of the hydration sites is decreased from five (P₀ system) to four (P₁₂₃ system). The hydration site H2 is substituted by the oxygen atom of V660 to coordinate Mg²⁺. The observation indicates that the presence of Mg²⁺-Mg²⁺ plays an important role in forming the Mg²⁺-coordination geometry, but which Mg²⁺ plays the major role in determining the conformation of Mg²⁺ binding site is still unclear. To address this, we compare the Mg²⁺-coordination geometry between Ago-Mg²⁺-Mg²⁺ (Fig. 5b) and Ago-Mg²⁺-Mg²⁺ (Fig. 5c). A comparison of P₁ and P₁₃ system shows that there is almost no difference between them, suggesting that Mg²⁺ may not make a contribution to the change of local conformation of Mg²⁺ binding site. Inspection of Fig. 5b shows that the geometry of Mg²⁺ is coordinated regularly by six oxygen atoms, four atoms come from water molecules and the other two atoms are provided by residues Q414 and V660. This observation is consistent with the geometry of Mg²⁺ in P₁₂₃ system. Interestingly, Mg²⁺-coordination geometry in P₁₂ system is similar to that in P₁ system, indicating that the presence of Mg²⁺ is the dominating contribution to the change of local conformation of Mg²⁺ binding region. We infer that Mg²⁺ enables to increase the fluctuation of the Ago protein globally, thus making residue V660 replace the H2 water molecule to form coordination bond with Mg²⁺, which is consistent with the results obtained from the plots of RMSD and the maps of cross correlation. After the binding of DNA-RNA (C₁₂ and C₁₃ systems), the geometry of Mg²⁺ is changed (Fig. 6e and f), the residue Q414 is far away from Mg²⁺ compared with the C₁ system (Fig. 5e), the phenomenon shows that the individual Mg²⁺ (the presence of Mg²⁺ or Mg²⁺) play a role in forming the local structure of Mg²⁺, indicating that the two Mg²⁺ (Mg²⁺ and Mg²⁺) presented at the same time may provide a better contribution for the interaction between the Ago protein and DNA-RNA. Then the Ago-Mg²⁺-Mg²⁺ system (Fig. 6a) and Ago-Mg²⁺ system (Fig. 6b), Ago-Mg²⁺-Mg²⁺ (Fig. 6c) and Ago-Mg²⁺ system (Fig. 6d) are compared to find the effect of the presence of Mg²⁺ on the Mg²⁺, Mg²⁺ coordination structures, notably, the same observation are obtained in the C₁₂ and C₁₃ systems. These results show that the geometries of Mg²⁺ and Mg²⁺ are constant at these systems, indicating that Mg²⁺ does not affect the Mg²⁺, Mg²⁺ coordination structures.

MM-GBSA calculation

In the above analysis, we have investigated how the binding of three Mg ions influences the interaction of the Ago protein with miRNA. To further validate our results and obtain more detailed information about the effects of Mg1, Mg2 and Mg3 on the interaction between DNA-RNA and Ago, we applied the MM-GBSA, a tool allowing the decomposition of electrostatic solvation free energy into atomic contributions in a straightforward way [35], to study the energetic implications of the contributions of the Mg²⁺ to the binding of DNA-RNA to Ago in the presence of solvent and thermal fluctuations. In this section, we have performed the relative free energy calculations of C₀ and C₁₂₃ (without the entropic calculation), with the Ago-Mg²⁺ as a receptor and the DNA-RNA as a ligand.

The total binding free energies of DNA-RNA binding to Ago in C₀ and C₁₂₃ system are $-148.54 \text{ kcal}\cdot\text{mol}^{-1}$ and $-192.55 \text{ kcal}\cdot\text{mol}^{-1}$, respectively, the $\Delta\Delta G$ between them is $-44.01 \text{ kcal}\cdot\text{mol}^{-1}$ (Table 1). This result reveals that the presence of the three Mg²⁺ ions favors the binding of DNA-RNA to Ago. To further study the contribution of each Mg²⁺ to the binding of DNA-RNA to Ago, the free energy decomposition is performed and the results are shown in Fig. 8.

The decomposed free energies of Mg1, Mg2 and Mg3 of C₁₂₃ system are -2.06 , -2.53 and $-1.94 \text{ kcal}\cdot\text{mol}^{-1}$, respectively, implying that the three magnesium ions are favorable for the binding of DNA-RNA to Ago. In order to understand how the magnesium ions contribute to the binding of DNA-RNA to Ago, the energy contributions of the residues/bases which create coordination bond with Mg²⁺ are taken into account. Figure 8 shows that the van de Waals interaction is the main driving force and the most favorable interaction lies in the nonpolar solvation. Residue Q414 and bases DT661 and DA663 surrounding the Mg1 contribute -4.15 , -7.82 and $-0.05 \text{ kcal}\cdot\text{mol}^{-1}$ to the binding of DNA-RNA to Ago, respectively. The high contribution of Q414 due to the indirect interaction with Mg1 [5], indicating that Mg1 works as a

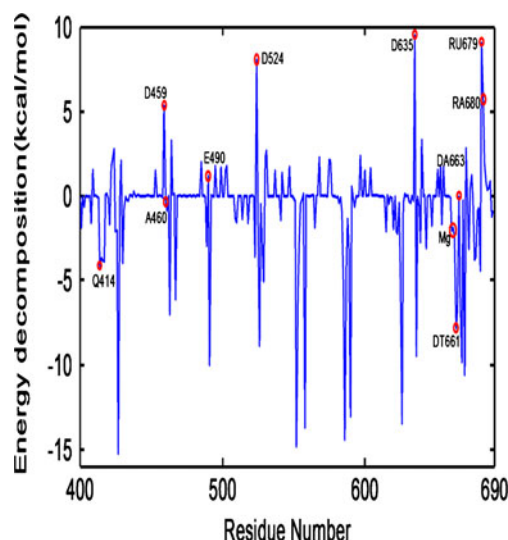


Fig. 8 Contribution of each individual residue of Ago, Mg²⁺ and each base of DNA-RNA in the C₁₂₃ system to the binding free energy. The key residues are marked with the red circle

media in the interface between the Ago protein and the guide DNA, eventually promoting the DNA-RNA to bind to Ago protein. In contrast, for A460, D524, D635, RA680 around Mg2, almost all the residues and the bases contribute unfavorably to the DNA-RNA binding, as evidenced by their energies of -0.27 , 8.05 , 9.5 and $5.77 \text{ kcal}\cdot\text{mol}^{-1}$, respectively. As for the residues surrounding Mg3, D459, E490 and D524 also contribute unfavorably to the binding of DNA-RNA with free energies of 5.32 , 1.16 and $8.05 \text{ kcal}\cdot\text{mol}^{-1}$, respectively. These results might be reasonable since the unfavorable contribution to the binding free energies is responsible for the cleavage of target RNA during RNA interference [49], which is validated by the analysis of cross-correlation maps in this work. In a word, the decomposition analysis of binding affinity of C₁₂₃ system provides us a complementary information about the mechanism by how the Mg²⁺ affects the structural dynamics of the complex and thus enhancing the binding/disassociation of DNA-RNA to the Ago protein.

Table 1 The free energy of DNA-RNA binding to Ago in C₀ and C₁₂₃ systems

Component ^a	C ₀		C ₁₂₃	
	Mean ^b (kcal/mol)	Std ^c	Mean ^b (kcal/mol)	Std ^c
ΔE_{vdw}	-296.96	14.03	-289.58	10.53
ΔE_{ele}	-2549.99	89.80	-4263.94	108.30
ΔG_{SOL}	2698.42	84.08	4360.97	91.52
ΔG	-148.54	19.93	-192.55	29.45

^a Energies shown as contributions from van der Waals energy (ΔE_{vdw}), electrostatic energy (ΔE_{ele}), solvation energy (ΔG_{SOL}), bind free energy (ΔG).^b Average over 100 snapshots. ^c Standard error of mean values

Conclusions

Mg²⁺ is known as a critical ion for the structure and biochemical properties of many RNAs and some ribozymes, while RNA-induced silencing complex (RISC) is a Mg²⁺-dependent endonuclease. Therefore it is important to probe the roles of Mg²⁺ on the miRNA recognized by Ago protein. In the present work, a series of sixteen 25 ns molecular dynamics simulations of Ago protein and Ago-DNA-RNA complex in the presence or absence of different Mg²⁺ are performed. For Mg1 and Mg2, their binding to Ago enhances the out-of-phase correlated motion of the PAZ, Mid and PIWI domain, resulting in the “open-closed” movement of the PAZ and the Mid,

PIWI domains. While the binding of Mg3 significantly decreases the motion of the whole Ago protein with the average RMSD of ~ 0.34 Å, compared with the systems in absence of Mg3 (average RMSD ~ 0.43 Å). Interestingly, the DNA-RNA seems to have a stronger impact on the protein global stability than that of Mg3. After the binding of DNA-RNA, a hydrogen bonding network is formed between the interfacial of Ago and DNA-RNA, which makes the global Ago protein more stable. In addition, the interaction of Mg^{2+} with the DNA-RNA is also probed by using free energy decomposition of MM-GBSA method, indicating that the three Mg^{2+} provide the favorable contribution to the binding of the DNA-RNA to the protein. Our models provide insights into the understanding of local and global effect of Mg^{2+} on the interaction between miRNA and Ago, which might be helpful in understanding the Ago-RNA- Mg^{2+} relationships and also provides useful information for the further investigation of the RNA interference pathway.

Acknowledgments The research is supported by high-performance computing platform of Northwest A & F University and the Fund of Northwest A & F University.

References

- Bartel DP (2009) MicroRNAs: target recognition and regulatory functions. *Cell* 136:215–230
- Bartel DP (2004) MicroRNAs: genomics, biogenesis, mechanism, and function. *Cell* 116:281–297
- Lee RC, Feinbaum RL, Ambros V (1993) The *C. elegans* heterochronic gene *lin-4* encodes small RNAs with antisense complementarity to *lin-14*. *Cell* 75:843–854
- Gregory RI, Chendrimada TP, Cooch N, Shiekhattar R (2005) Human RISC couples microRNA biogenesis and posttranscriptional gene silencing. *Cell* 123:631–640
- Wang YL, Juranek S, Li HT, Sheng G, Tuschl T, Patel DJ (2008) Structure of an argonaute silencing complex with a seed-containing guide DNA and target RNA duplex. *Nature* 456:18–25
- Wang X, Li Y, Xu X, Wang Y (2010) Toward a system-level understanding of microRNA pathway via mathematical modeling. *Biosystems* 100:31–38
- Zhou W, Li Y, Wang X, Wu LQ, Wang YH (2011) MiR-206-mediated dynamic mechanism of the mammalian circadian clock. *BMC Syst Biol* 5:41
- Wang X, Xu X, Ma Z, Huo YQ, Xiao ZT, Li Y, Wang YH (2011) Dynamic mechanisms for pre-miRNA binding and export by Exportin-5. *RNA* 17:1511–1528
- Wang YH, Li Y, Ma Z, Yang W, Ai CZ (2010) Mechanism of MicroRNA-target interaction: molecular dynamics simulations and thermodynamics analysis. *PLoS Comput Biol* 6(7)
- Song JJ, Smith SK, Hannon GJ, Joshua-Tor L (2004) Crystal structure of Argonaute and its implications for RISC slicer activity. *Science* 305:1434–1437
- Bernstein E, Caudy AA, Hammond SM, Hannon GJ (2001) Role for a bidentate ribonuclease in the initiation step of RNA interference. *Nature* 409:363–366
- Song JJ, Joshua-Tor L (2006) Argonaute and RNA-getting into the groove. *Curr Opin Struct Biol* 16:5–11
- Song JJ, Liu JD, Tolia NH, Schneiderman J, Smith SK, Martienssen RA, Hannon GJ, Joshua-Tor L (2003) The crystal structure of the Argonaute2 PAZ domain reveals an RNA binding motif in RNAi effector complexes. *Nat Struct Biol* 10:1026–1032
- Lingel A, Simon B, Izaurralde E, Sattler M (2004) Nucleic acid 3'-end recognition by the Argonaute2 PAZ domain. *Nat Struct Mol Biol* 11:576–577
- Ma JB, Ye K, Patel DJ (2004) Structural basis for overhang specific small interfering RNA recognition by the PAZ domain. *Nature* 429:318–322
- Lingel A, Simon B, Izaurralde E, Sattler M (2003) Structure and nucleic-acid binding of the *Drosophila* Argonaute2 PAZ domain. *Nature* 426:465–469
- Yan KS, Yan S, Farooq A, Han A, Lei Z, Zhou MM (2003) Structure and conserved RNA binding of the PAZ domain. *Nature* 426:469–474
- Schwarz DS, Tomari Y, Zamore PD (2004) The RNA-induced silencing complex is a Mg^{2+} -dependent endonuclease. *Curr Biol* 14:787–791
- Draper DE, Grilley D, Soto AM (2005) Ions and RNA folding. *Annu Rev Biophys Biomol Struct* 34:221–243
- Michael JC, Shi YX, Latifi T, Eduardo AG (2006) An RNA sensor for intracellular Mg^{2+} . *Cell* 125:71–84
- Misra VK, Draper DE (2002) The linkage between magnesium binding and RNA folding. *J Mol Biol* 317:507–521
- Misra VK, Draper DE (1998) On the role of magnesium ions in RNA stability. *Biopolymers* 48:113–135
- Fedor MJ (2002) The role of metal ions in RNA catalysis. *Curr Opin Struct Biol* 12:289–295
- Lee TS, López CS, Giambasù GM, Martick M, Scott WG, York DM (2008) Role of Mg^{2+} in hammerhead ribozyme catalysis from molecular simulation. *J Am Chem Soc* 130:3053–3064
- Guex N, Peitsch MC (1997) SWISS-MODEL and the swiss-PdbViewer: an environment for comparative protein modeling. *Electrophoresis* 18:2714–2723
- DeLano WL (2002) The PyMOL Molecular Graphics System. DeLano Scientific, San Carlos, CA, USA
- Berendsen HJC, van der Spoel D, van Drunen R (1995) GROMACS: a message-passing parallel molecular dynamics implementation. *Comput Phys Commun* 91:43–56
- Wang J, Cieplak P, Kollman PA (2000) How well does a restrained electrostatic potential (RESP) model perform in calculating conformational energies of organic and biological molecules? *J Comput Chem* 21:1049–1074
- Jorgensen WL, Chandrasekhar J, Madura JD, Impey RW, Klein ML (1983) Comparison of simple potential functions for simulating liquid water. *J Chem Phys* 79:926–935
- Bussi G, Donadio D, Parrinello M (2007) Canonical sampling through velocity rescaling. *J Chem Phys* 126:014101
- Darden T, York D, Pedersen L (1993) Particle mesh Ewald: an Nlog(N) method for Ewald sums in large systems. *J Chem Phys* 98:10089–10092
- Hess B, Bekker H, Berendsen HJC, Fraaije JGEM (1997) LINCS: a linear constraint solver for molecular simulations. *J Comput Chem* 18:1463–1472
- Ichiye T, Karplus M (1991) Collective motions in proteins: a covariance analysis of atomic fluctuations in molecular dynamics and normal mode simulations. *Prot Struct Funct Genet* 11:205–217
- Swaminathan S, Harte WE Jr, Beveridge DL (1991) Investigation of domain structure in proteins via molecular dynamics simulation: application to HIV-1 protease dimmer. *J Am Chem Soc* 113:2717–2721
- Kollman PA, Massova I, Reyes C, Kuhn B, Huo S, Lee M, Lee T, Duan Y, Wang W, Donini O, Cieplak P, Srinivasan J, Case DA, Cheatham TE III (2000) Calculating structures and free energies of complex molecules: combining molecular mechanics and continuum models. *Acc Chem Res* 33:889–897

36. Case DA, Cheatham TE, Darden T, Gohlke H, Luo R, Merz KM Jr, Onufriev A, Simmerling C, Wang B, Woods RJ (2005) The Amber biomolecular simulation programs. *J Comput Chem* 26:1668–1688
37. Wagoner JA, Baker NA (2006) Assessing implicit models for nonpolar mean solvation forces: the importance of dispersion and volume terms. *Proc Natl Acad Sci U S A* 103:8331–8336
38. Sanner MF, Olson AJ, Spehner JC (1996) Reduced surface: an efficient way to compute molecular surfaces. *Biopolymers* 38:305–320
39. Still WC, Tempczyk A, Hawley RC, Hendrickson T (1990) Semi-analytical treatment of solvation for molecular mechanics and dynamics. *J Am Chem Soc* 112:6127–6129
40. Gohlke H, Kiel C, Case DA (2003) Insights into protein–protein binding by binding free energy calculation and free energy decomposition for the Ras-Raf and Ras-RalGDS complexes. *J Mol Biol* 330:891–913
41. James SP (2010) How to slice: snapshots of Argonaute in action. *Silence* 1:3
42. Kim H, Jeong E, Lee SW, Han K (2003) Computational analysis of hydrogen bonds in protein-RNA complexes for interaction patterns. *FEBS Lett* 552:231–239
43. Conaco C, Otto S, Han JJ, Mandel G (2006) Reciprocal actions of REST and a microRNA promote neuronal identity. *Proc Natl Acad Sci U S A* 103:2242–2247
44. Tarek M, Tobias DJ (2000) The dynamics of protein hydration water: a quantitative comparison of molecular dynamics simulations and neutron-scattering experiments. *Biophys J* 79:3244–3257
45. Long ZR, Yang PJ, Xia YN, Yang ZW, Wu B (2009) A new sulfonamide derivative as magnesium ion receptor: N-tosyl-2,6-diisopropyl-4-(2,3-dimethoxybenzoylamide)aniline. *Tetrahedron Lett* 50:1820–1824
46. Vrbka L, Mucha M, Minofar B, Jungwirth P, Brown EC, Tobias DJ (2004) Propensity of soft ions for the air/water interface. *Curr Opin Colloid Interface Sci* 9:67–73
47. Hutvagner G, Simard MJ (2008) Argonaute proteins: key players in RNA silence. *Nat Rev Mol Cell Biol* 9:22–32
48. Martinez J, Tuschl T (2004) RISC is 5' phosphomonoester producing RNA endonuclease. *Gen Dev* 18:975–980
49. Liu J, Carmell MA, Rivas FV, Marsden CG, Thomson JM, Song JJ, Hammond SM, Joshua-Tor L, Hannon GJ (2004) Argonaute2 is the catalytic engine of mammalian RNAi. *Science* 305:1437–1441